ISSN 8755-6839

SCIENCE OF **TSUNAMI HAZARDS**

Journal of Tsunami Society International

Volume 37 **Number 1** **2018**

QUANTITATIVE STUDIES ABOUT TSUNAMI GENERATION AND PROPAGATION WAVES BY A STOCHASTIC SUBMARINE SLUMP AND LANDSLIDE SOURCE MODEL

Khaled T. Ramadan

Department of Basic and Applied Sciences, College of Engineering and Technology, Arab Academy for Science, Technology and Maritime Transport, P.O. Box 1029, Abu Quir Campus, Alexandria, Egypt.
kramadan@aast.edu

ABSTRACT

Tsunami generation and propagation due to a vertical time-dependent extent of a stochastic submarine slump and landslide model for different values of Froude number and noise intensity are investigated. The critical parameters controlling the oscillations and the amplitude of the free surface elevation are through the Froude number and the noise intensity induced by the stochastic submarine slump and landslide source model. Quantitative information about the tsunami generation and propagation waves will be provided by estimating the evolution of the displaced water volume, the potential, kinetic and total energy of the resulting waves and the averaged tsunami velocity components at different Froude numbers. The inclusion of the random noise of the submarine slump and landslide deformation provided an additional and a noticeable contribution to the quantitative characteristics of the free surface elevation.

Keywords: Tsunami waves, tsunami energy, velocity flow rate, water displacement, submarine slump and landslide, stochastic process.

1. INTRODUCTION

Tsunami waves generated by submarine landslides may be triggered by earthquakes, by volcanic eruptions, by storm waves, or may be initiated by gravitational loading and instability, and are particularly devastating in the near-field region, producing locally extremely large amplitude waves and run-up for coastal communities (Jiang, L. and LeBlond, 1992, 1994).

Submarine landslides might be locally much stronger and ravaging than the earthquake-induced waves producing major potential hazard, offering little time for warning due to their proximity to shore. Any type of geophysical mass flow events which encompasses a wide range of ground movement such as debris flows, debris avalanches, rock and soil falls can create submarine landslides which generate tsunamis (Yavari-Ramshe and Ataie-Ashtiani, 2016). Catastrophic tsunami events due to submarine landslides such as the Flores Island 1992(Imamura et al., 1995; Bardet et al., 2003), Storegga Slide (Harbitz 1992; Bondevik et al. 2005), Papua New.Guinea 1998 (Synolakis et al., 2002, Tappin et al., 2008), the tsunami in Izmit Bay (Turkey) of 17 August 1999 (Watts et al., 2005), the tsunami in Fatu Hiva, Marquesas islands, French Polynesia, of 13 September 1999 (Okal et al., 2002), the Stromboli tsunami of 30 December 2002 (Tinti et al., 2006), the possible landslide tsunami of 7 May 2007 in the Black Sea (Ranguelov et al., 2008), and the largest known tsunami event in Lituya Bay, Alaska of 9 July 1958 (Fritz et al., 2009), caused widespread damage and loss of life and hence have significantly increased an interest in studying landslide generated tsunamis.

A sudden upward or downward motion of a portion of the ocean floor will displace a large amount of water and generate a tsunami. A tsunami source of energy can be described by the water displacement event. It has been long known that large landslides can displace significant volumes of water and thus cause locally large tsunami waves. Fritz et al. (2003) discussed the landslide impact induced water displacement volume and concluded that the maximum crater volume, which corresponds to the water displacement volume, exceeded the landslide volume by up to an order of magnitude. Ruff (2003) stated that for landslides, the best way for measuring the displaced water volume is through the total material volume, or total distance traveled, or some combination of these two parameters. Satake and Tanioka (2003) computed the displaced water volume from different source models and compared with the displaced water volume at 1998 Papua New Guinea earthquake. They concluded that the far-field tsunami amplitudes are proportional to the displaced water volume at the source, while the near-field tsunami surface elevations are determined by the potential energy of the displaced water. Hassan et al. (2010) studied the maximum tsunami amplitudes for different lengths and widths of a submarine slump and slide source model and concluded that the amplification of the waveforms depends on the volume of the displaced water by the moving submarine landslide which became an important factor in the modeling of the tsunami generation.

Ocean bottoms are indeed far from being flat and smooth. The presence of fluctuations in the sources of tsunamis can cause unexpectedly strong fluctuations in the wave height of tsunamis, with maxima several times higher than the average wave height (Degueldre et al. 2016). The complexity of the geologic processes responsible for the depth profile of the ocean floor makes it natural to describe the bathymetry as a correlated random medium. The best way to show their aspects is through heterogeneous or stochastic source models. Numerous studies have been conducted to describe the entire process of tsunami events generated caused by submarine earthquakes, taken into account the random components of bottom deformation in tsunami simulation, see Geist (2002, 2005, 2013, 2016); Omar et al., (2012, 2014, 2016);

Ramadan (2014); Allam et al. (2014); Fukutani et al. (2015); Ruiz et al. (2015) and Ramadan et al. (2017), and by random components of submarine landslides, see Dutykh et al. (2013); Dias et al. (2014) and Ramadan et al. (2014, 2015).

Forecasting tsunami events and providing timely evacuation warnings to communities is one of the most effective ways to reduce the loss of human lives and the damage to communities. The total energy transmitted by tsunami waves is one of the most fundamental quantities for quick estimation of the potential impact of a tsunami (Bernard and Titov 2015). The energy release is probably the best relative measure of earthquake and landslide size. Numerous studies have been examined the energy transmitted by the tsunami waves caused by underwater earthquakes (see, Dutykh et al. 2012, Tang et al. 2012, Jamin et al. 2015, Ramadan et al. 2017). During submarine mass movements, energy is invested in the displacement of the surrounding water. This might lead to the initiation of a series of tsunami waves that propagate towards the coast. Tinti and Bortolucci (2000) analyzed energy transmission from a submarine landslide to a water body using 1D and 2D shallow-water wave models. Dutykh and Dias (2009) investigated the energy of waves generated by bottom motion in the framework of the nonlinear SWEs, for both dispersive and non-dispersive waves and in the framework of the dispersive linearized equations. Zhao et al. (2012) obtained the energy transformation over a uniform sloping beach in terms of the reconstruction of the full velocity field by Boussinesq equations. Ma et al. (2015) conducted a wave energy analysis to investigate how the deformable landslide transfers energy to the surface waves and illustrated the potential and kinetic energies of the impulse wave generation for granular landslide motion. López-Venegas et al. (2015) studied the total energy of the water induced by the submarine landslide in the system (3D–2D coupled models). They concluded that most of the wave energy is isolated in the wave generation region, particularly at depths near the landslide. Whittaker et al. (2015) studied experimentally the effect of the submarine landslide Froude number on the potential energy time series within the wave field. McFall and Fritz (2016) measured the wave train energy, generated by a gravel landslide on planar and convex conical hill slopes.

The tsunami flow velocity is a significant physical parameter to understand tsunami behaviors. To measure, predict, and compute tsunami flow velocities is of importance in risk assessment and hazard mitigation which may provide a clear signal of tsunami flows, where the arrival of the tsunami is indicated by the commencement of distinctive current velocity oscillations (Lipa et al. 2012). This enables us to visualize the tsunami generation process, including the velocity components. Several studies have inferred current velocities from analysis of tsunami deposits. Choowong et al. (2008) estimated a depth-averaged flow velocity ranging between 7-21 m/s from the thickness and grain size of sediment deposited by the 2004 Indian Ocean tsunami in Phuket, Thailand. Didenkulova et al. (2010) presented a linear shallow-water theory for tsunami wave generation by underwater landslides with depth averaged flow velocity. Lipa el al. (2012) measured the orbital velocity components to observe the tsunami signal in HF radar. They formed a time series of the average velocity, which shows the characteristic oscillations produced by the tsunami. Ma et al. (2013) presented the time series of surface horizontal velocities induced by submarine landslides and compared normalized velocity profiles at both supercritical and subcritical regions by the layer-averaged velocity. Lin et al. (2015) showed the velocity field near a moving landslide at different time values.

The objective of this study is to illustrate tsunami distributions predicted in the near-and far-field caused by a dynamic displacement of a stochastic submarine slump and landslide for different values of Froude number and noise intensity. Stochastic effects have been incorporated by including two Gaussian white

noise processes in the x– and y–direction to form the stochastic source model. Wave gauges are represented at different locations, in order to make a contribution to the improvement the warning system of tsunami arrival. Of particular interest in this study is to represent the displaced water volume as a result of the stochastic submarine slump and landslide, the potential, kinetic and total energy of the free surface elevation and the surface average velocity flow rates during the generation and propagation processes under the effect of different Froude numbers. The problem is solved using the linearized water wave theory for constant water depth by transforming methods (Laplace in time and Fourier in space), with the forward and inverse Laplace transforms solved analytically, and the inverse Fourier transform computed numerically by the Inverse Fast Fourier Transform (IFFT).

The present study is organized as follows. Section 2 presents the mathematical formulation of the linear water wave problem. It also presents the mathematical description of the stochastic submarine slump and landslide. Section 3 presents the tsunami analysis results caused by the stochastic submarine slump and landslide. The time-evolution during tsunami generation and propagation is described in Section 3.1. Section 3.2 presents the displace water volume and the tsunami energy. Section 3.3 presents the average velocity time series. Finally, Section 4 provides the main conclusions of this study.

2. MATHEMATICAL FORMULATION OF THE LINEAR WATER WAVE PROBLEM

It is considered that the fluid is incompressible and the flow is irrotational in the fluid domain $\Omega = R^2 \times [-h, 0]$ bounded above by the free surface of the ocean $z = \eta(x, y, t)$ and below by the rigid ocean floor $z = -h + \zeta(x, y, t)$ as shown in Fig. 1, where $\eta(x, y, t)$ is the free surface elevation, h is the constant water depth and $\zeta(x, y, t)$ is the sea floor displacement function.

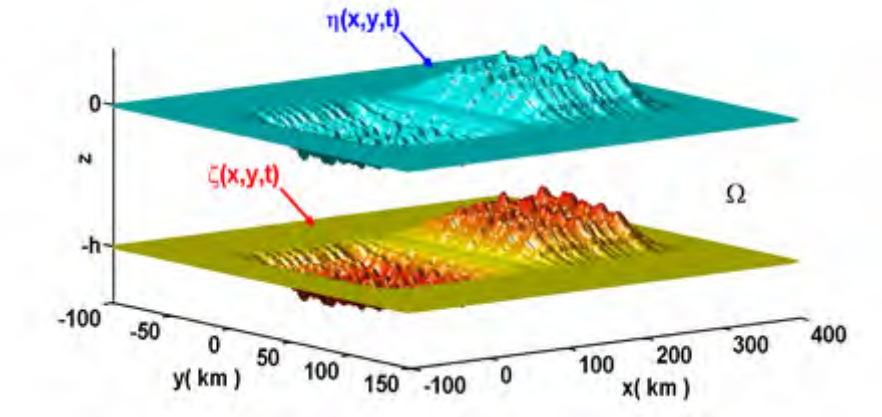

Figure 1. Fluid domain and coordinate system for a very rapid movement of the stochastic submarine slump and landslide model

The linearized problem can be expressed in terms of the velocity potential $\phi(x, y, z, t)$ by the Laplace equation as:

$$\nabla^2\phi(x, y, z, t) = 0 \text{ where } (x, y, z) \in \Omega, \tag{1}$$

subjected to the following boundary conditions

$$\partial_z\phi(x, y, z, t)\Big|_{z=0} = \partial_t\eta(x, y, t), \tag{2}$$

$$\partial_z\phi(x, y, z, t)\Big|_{z=-h} = \partial_t\zeta(x, y, t), \tag{3}$$

and

$$\partial_t\phi(x, y, z, t)\Big|_{z=0} + g\,\eta(x, y, t) = 0. \tag{4}$$

where g is the acceleration due to gravity. The initial conditions are given as

$$\phi(x, y, z, 0) = \eta(x, y, 0) = \zeta(x, y, 0) = 0. \tag{5}$$

The linear water wave theory has been developed as a fundamental theory in questions of stability for both near– and far–field problem in the open ocean which provides an ample understanding of the physical characteristics of the tsunami, see, Kervella et al (2007); Saito and Furumura (2009); Constantin and Germain (2012); Saito (2013) and Jamin et al. (2015). Additionally, one of the notable consequences of the linear theory is that the height distribution at the surface is not always identical to the bottom, see Jamin et al. (2015) and Saito (2013). Nonlinear effects become significant and dominant as tsunami enters the run-up phase, see Lynett and Liu (2002); Glimsdal et al. (2007); Løvholt et al. (2012) and Samaras et al. (2015).

We applied the transform methods (Laplace in time and Fourier in space) to solve analytical the linearized problem of the long traveling free surface elevation, η, in the open ocean during the generation and propagation processes for constant water depth, h at resonance state (when, $v = v_t = \sqrt{gh}$, i.e. maximum amplification, see Ramadan et al. (2011) . This solution is accurate if the depth of the water, h, is much greater than the amplitudes of and ζ (sea floor uplift) and η (free surface elevation) and if the wavelength of the leading wave of the incoming tsunamis is very long in comparison with the local water depth, which is usually true for most tsunamis triggered by submarine earthquakes, slumps and slides, see Todorovska and Trifunac (2001); Trifunac et al. (2002a, 2002b); Todorovska et al. (2002); Trifunac et al. (2003); Hayir (2006) and Jamin et al. (2015). All these studies neglected the nonlinear terms in the boundary conditions to study the generation of the tsunami waves using the transform methods.

In this paper, an analytical approach was used to illustrate the tsunami wave, the displaced water volume as a result of the submarine slump and landslide, the potential and kinetic energy of the free surface elevation and the average velocity flow rates in the open ocean during the generation and propagation processes for a given stochastic submarine slump and landslide profile $\zeta(x, y, t)$ for different Froude numbers. All our studies took into account constant depths h for which the Laplace and Fast Fourier

Transform (FFT) methods could be applied. After applying the Fourier–Laplace transform of the Laplace equation (1) and the boundary conditions (2) – (4), and using the initial conditions in (5), the velocity potential $\bar{\phi}\left(k_1, k_2, z, s \right)$ and the free surface elevation $\bar{\eta}\left(k_1, k_2, s\right)$ are obtained, respectively as seen in Ramadan et al. (2015) as:

$$\bar{\phi}\left(k_1, k_2, z, s \right) = -\frac{gs\,\bar{\zeta}\left(k_1, k_2, s \right)}{\cosh\left(kh\right)\left(s^2 + \omega^2\right)}\left(\cosh\left(kz\right) - \frac{s^2}{gk}\sinh(kz)\right), \tag{6}$$

and

$$\bar{\eta}\left(k_1, k_2, s \right) = \frac{s^2\,\bar{\zeta}\left(k_1, k_2, s \right)}{\cosh\left(kh\right)\left(s^2 + \omega^2\right)}\ . \tag{7}$$

where $\omega = \sqrt{gk\tanh\left(kh\right)}$ is the gravity-wave dispersion relation and $k = \sqrt{{k_1}^2 + {k_2}^2}$ is the wavenumber.

A solution for $\eta\left(x, y, t\right)$ can be obtained from equation (7) by performing the inverse transforms. The above linearized solution is known as the linear water solution. The mechanism of the tsunami generation caused by submarine gravity mass flows is initiated by a rapid down and uplift faulting as shown in Fig. 2, then propagated randomly in the positive $x-$ direction with time $0 \le t \le t^*$, to a length L with velocity v to produce an accumulation and depletion zones as shown in Fig. 3. In the $y-$direction, the model propagates instantaneously during the time $0 \le t \le t^*$.The set of physical parameters used in the problem are given in Table 1.

Table 1 Parameters used in the analytical solution of the problem

Parameters	Values for the submarine slump and landslide
-Source width, D , km	50
- propagated length L, km	100
-Water depth (uniform), h, km	2
-Acceleration due to gravity, g, km/sec^2	0.0098
-Tsunami phase velocity, $v_t = \sqrt{gh}$, km/sec	0.14
- submarine velocity (at resonance) $v = v_t$, km/sec	0.14
- Characteristic time t* (at resonance) $t^* = \frac{L}{v} = 714\ \text{sec} = 11.9\ \text{min}$	

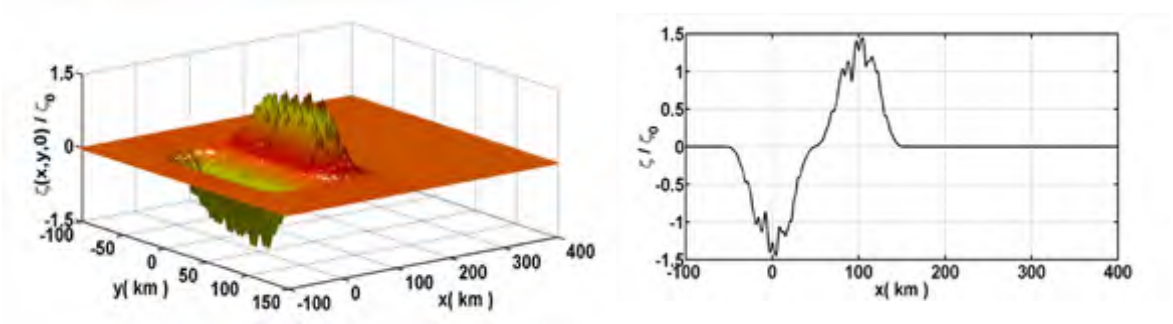

Figure 2. Normalized initial bottom topography representing by a stochastic down and uplift faulting (a) Three−dimensional view (b) Side view

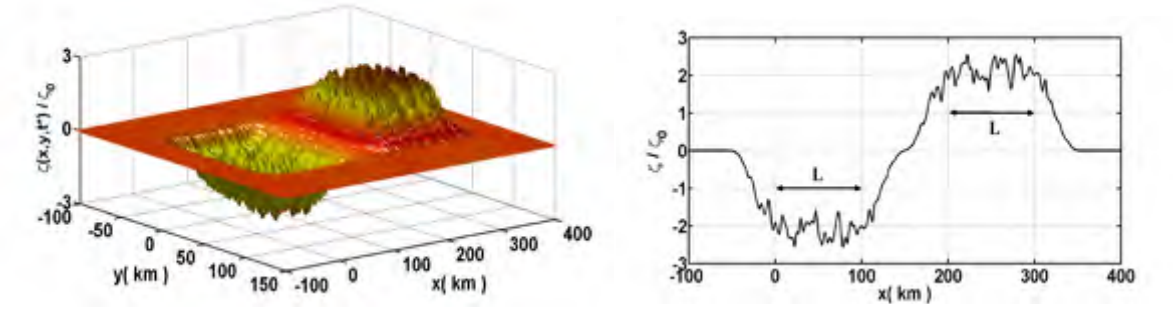

Figure 3. Normalized Bed deformation model representing by a random accumulation and depletion zones at $t = t^* = L/v = 100/v$ (a) Three−dimensional view (b) Side view.

Modeling tsunamis generated by submarine slumps and landslides requires modeling the landslide motion. The dynamic stochastic submarine slump and landslide model shown in Fig. 3 for $0 \le t \le t^*$ is given by:

$$\zeta_{down}(x,y,t) = \left[\zeta_{1down}(x,y,t) + \zeta_{2down}(x,y,t) + \zeta_{3down}(x,y,t)\right]\left(1 + \sigma_x\xi_x(x+50) + \sigma_y\xi_y(y+50)\right) \quad (8)$$

for $-50 \le x \le 50+ vt$ and $-50 \le y \le 100$.

For $y \in [-50,0]$

$$\zeta_{1down}(x,y,t) = \begin{cases} -\frac{\zeta_0}{4}\left(1 + \cos\frac{\pi}{50}x\right)\left[1 - \cos\frac{\pi}{50}(y+50)\right], & -50 \le x \le 0, \\ -\frac{\zeta_0}{2}\left[1 - \cos\frac{\pi}{50}(y+50)\right], & 0 \le x \le vt, \\ -\frac{\zeta_0}{4}\left[1 + \cos\frac{\pi}{50}(x - vt)\right]\left[1 - \cos\frac{\pi}{50}(y+50)\right], & vt \le x \le 50+ vt, \end{cases} \quad (9)$$

and for $y \in [0, 50]$

$$\zeta_{2down}(x,y,t)=\begin{cases}-\frac{\zeta_0}{2}\left(1+\cos\frac{\pi}{50}x\right), & -50\le x\le 0,\\ -\zeta_0, & 0\le x\le vt,\\ -\frac{\zeta_0}{2}\left[1+\cos\frac{\pi}{50}(x-vt)\right], & vt\le x\le 50+vt,\end{cases} \tag{10}$$

and for $y\in[50,100]$

$$\zeta_{3down}(x,y,t)=\begin{cases}-\frac{\zeta_0}{4}\left(1+\cos\frac{\pi}{50}x\right)\left[1+\cos\frac{\pi}{50}(y-50)\right], & -50\le x\le 0,\\ -\frac{\zeta_0}{2}\left[1+\cos\frac{\pi}{50}(y-50)\right], & 0\le x\le vt,\\ -\frac{\zeta_0}{4}\left[1+\cos\frac{\pi}{50}(x-vt)\right]\left[1+\cos\frac{\pi}{50}(y-50)\right], & vt\le x\le 50+vt.\end{cases} \tag{11}$$

$$\zeta_{up}(x,y,t)=\left[\zeta_{1up}(x,y,t)+\zeta_{2up}(x,y,t)+\zeta_{3up}(x,y,t)\right]\left(1+\sigma_x\xi_x(x-50-vt)+\sigma_y\xi_y(y+50)\right), \tag{12}$$

for $50+vt\le x\le 150+2vt$ and $-50\le y\le 100$.

For $y\in[-50,0]$

$$\zeta_{1up}(x,y,t)=\begin{cases}\frac{\zeta_0}{4}\left[1+\cos\frac{\pi}{50}(x-vt)\right]\left[1-\cos\frac{\pi}{50}(y+50)\right], & 50+vt\le x\le 100+vt,\\ \frac{\zeta_0}{2}\left[1-\cos\frac{\pi}{50}(y+50)\right], & 100+vt\le x\le 100+2vt,\\ \frac{\zeta_0}{4}\left[1+\cos\frac{\pi}{50}(x-(100+2vt))\right]\left[1-\cos\frac{\pi}{50}(y+50)\right], & 100+2vt\le x\le 150+2vt\end{cases} \tag{13}$$

and for $y\in[0,50]$

$$\zeta_{2up}(x,y,t)=\begin{cases}\frac{\zeta_0}{2}\left[1+\cos\frac{\pi}{50}(x-vt)\right], & 50+vt\le x\le 100+vt,\\ \zeta_0, & 100+vt\le x\le 100+2vt,\\ \frac{\zeta_0}{2}\left[1+\cos\frac{\pi}{50}(x-(100+2vt))\right], & 100+2vt\le x\le 150+2vt,\end{cases} \tag{14}$$

and for $y\in[50,100]$

$$\zeta_{3up}(x,y,t)=\begin{cases}\frac{\zeta_0}{4}\left[1+\cos\frac{\pi}{50}(x-vt)\right]\left[1+\cos\frac{\pi}{50}(y-50)\right], & 50+vt\le x\le 100+vt,\\ \frac{\zeta_0}{2}\left[1+\cos\frac{\pi}{50}(y-50)\right], & 100+vt\le x\le 100+2vt,\\ \frac{\zeta_0}{4}\left[1+\cos\frac{\pi}{50}(x-(100+2vt))\right]\left[1+\cos\frac{\pi}{50}(y-50)\right], & 100+2vt\le x\le 150+2vt,\end{cases}$$

(15)

where ζ_0 denotes the initial uplift of the smooth bottom topography, $\xi_x(x)$ and $\xi_y(y)$ denote two independent Gaussian white noise processes which are random processes with two real valued parameters σ_x , $\sigma_y \ge 0$ that control the strength of the induced noise in the x− and y−directions, respectively and v is the spreading velocity of the stochastic bottom in the x−direction.

The deformation of the random submarine slump and landslide shown in Fig. 3 could represent the slide with mass movement in the down slope direction, see Fig. 3 in Normark et al. (1993) and the three-dimensional bathymetry of the sea floor north of Puerto Rico, see Fig. 2 in Schwab et al. (1993) and Fig. 1(b) in Brink et al. (2006). So, the evidence of a huge historical tsunami need for investigating the possibility of future tsunami generating by stochastic submarine slumps and landslides.

The considered stochastic submarine slump and landslide source model is spreading unilateral in the x-direction as shown in Fig. 4 where the vertical displacement is negative (downwards) in zone of depletion, and positive (upwards) in zone of accumulation. The schematic representation of the submarine slump and landslide shown in Fig. 4 resembles the debris flow model in Fig. 1 (bottom left) in Løvholt et al. (2017). For $t \ge t^*$ (propagation process), $\zeta_{down}(x,y,t)$ and $\zeta_{up}(x,y,t)$ are the same as (8) and (12) except the time parameter t will be substituted by t*.

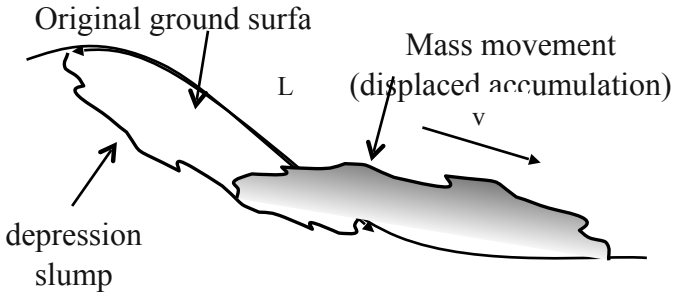

Figure 4. Schematic representation of the kinematic submarine landslide travelling a significant distance L downhill creating a depression slump and a displaced accumulation mass movement spreading uphill with velocity v.

Laplace and Fourier transforms can now applied to the bed motion described by Equations (8) and (12), then substituting into (7) and then inverting $\bar{\eta}(k_1,k_2,s)$ using the inverse Laplace transform and the double inverse Fourier transform to obtain $\eta(x,y,t)$, see Ramadan et al. (2015).

To evaluate the horizontal velocity components along the free surface (z = 0) denoted by **u** (U, V), and the horizontal gradient ($\frac{\partial}{\partial x}, \frac{\partial}{\partial y}$) denoted by ∇_h, and the Fourier transform parameters denoted $\mathbf{m} = (k_1, k_2)$, hence the horizontal components of the velocity are defined as:

$$\mathbf{u}(x, y, t) = \nabla_h \phi(x, y, t) , \tag{16}$$

taking into account that the horizontal velocities are independent of the vertical coordinate, z. The Fourier transforms of the horizontal components taken along the absolute value of the free surface η in case of slump and slide for $0 \le t \le t^*$ (generation process) are given as:

$$\bar{\mathbf{u}}(k_1, k_2, t) = -i\bar{\phi}(k_1, k_2, t)\mathbf{m} ,$$

$$= i\left[g\int_0^t \left|\bar{\eta}(k_1, k_2, \tau)\right| d\tau \right]\mathbf{m} . \tag{17}$$

For $t \ge t^*$ (propagation process), the integration $\int_0^t \left|\bar{\eta}(k_1, k_2, \tau)\right| d\tau$ in equation (17) is written as $\int_0^{t^*} \left|\bar{\eta}(k_1, k_2, \tau)\right| d\tau + \int_{t^*}^t \left|\bar{\eta}(k_1, k_2, \tau)\right| d\tau$.

The surface average velocity flow rates are given as $\bar{u} = \frac{Q_x}{\iint dxdy}$ and $\bar{v} = \frac{Q_y}{\iint dxdy}$, where $Q_x = \iint U dxdy$ and $Q_y = \iint V dxdy$ are called volume flow rates.

We are interested in representing the displaced water volume, the potential and kinetic energies of the tsunami wave due to vertical displacement of the stochastic submarine slump and landslide model in the near- and far-field under the effect of the Froude number to investigate for the tsunami wave amplification and the potential for tsunami generation and propagation.

The volume of water displaced as a result of the submarine slump and landslide can be determined as the integral of the absolute value of the function η taken over the entire tsunami source area. Then the total displaced water volume V(t) is given as :

$$V(t) = \int_{R^2} \left|\eta\right| dxdy . \tag{18}$$

The accumulated kinetic energy, $E_K(t)$ generated by the movement of the water particles of the mass flow imparted to the flow region and the accumulated potential energy, $E_p(t)$ induced by the displacement of the free surface from the mean position, can be evaluated at any time by integration over the whole deformation area as (see Ramadan et al., 2017):

$$E_K(t) = \frac{1}{2}\rho \int_{R^2}\int_{-h}^{\eta} \left|\nabla\phi\right|^2 dzdxdy = \frac{1}{2}\rho \int_{R^2}\int_{-h}^{\eta} \left(U^2 + V^2 + W^2\right) dzdxdy , \tag{19}$$

and $$E_p(t) = \int_{R^2} \int_0^{|\eta|} \rho g z \, dz dx dy = \frac{1}{2} \rho g \int_{R^2} |\eta|^2 dx dy \ , \quad (20)$$

where $\rho = 1000\ kg/m^3$ is the water density, U and V are the horizontal water velocity fields within the range of R_x and R_y , respectively and W is the vertical velocity field due the seafloor uplift. Taken together, we obtained the total energy $E_T(t) = E_p(t) + E_K(t)$. Both horizontal and vertical velocities are taken into account, so the conservation of total wave energy is well satisfied (Dutykh and Dias 2009). It is assumed that the initial energy of the tsunami is purely potential, by hypothesis the initial kinetic energy is null and hence the initial velocities are also null.

3. RESULTS AND DISCUSSIONS

Modeling submarine landslide -triggered tsunami generation and propagation is now standard for hazard analysis of vulnerable coastlines. The tsunami generation and propagation are illustrated by a vertical time-dependent displacement of a stochastic mass failure model driven by two Gaussian white noise processes in the x– and y–directions. The numerical results demonstrate the waveform in the near-field resulting from the stochastic slump and landslide elongation to one direction (length) that vertically displaces the water column, and the wave amplitudes decaying, due to geometric spreading and dispersion in the far−field. The displaced water volume, the tsunami potential and kinetic energy and the average surface velocities induced by the stochastic submarine slump and landslide source model for different Froude numbers are illustrated in the near− and far−field.

3.1 Time-Evolution during Tsunami Generation and Propagation

Submarine slumps and landslides that produce vertical displacement change the shape of the ocean basin, which affect the entire water column and generate a tsunami. The ratio of the submarine landslide speed to the local phase velocity of the free water waves in water depth h, is known as Froude number and plays a fundamental role in determining the generation and evolution of the induced tsunami (Tinti and Bortolucci, 2000).

Figure 5 presents the top view of the stochastic slump and slide source model at $t^* = L/v$, showing the location of four selected gauges. We chose the locations of these gauges based on different altitudes of the stochastic slump and landslide source model. Wave gauges are used to measure the wave height for different values of Froude number. Observations were made on water level at the four locations, (50, 25), (78, 42), (250, 25) and (278, 42). The measurement points were chosen as a reference point for evaluating the effects of enlargement in the flow of the tsunami generation level.

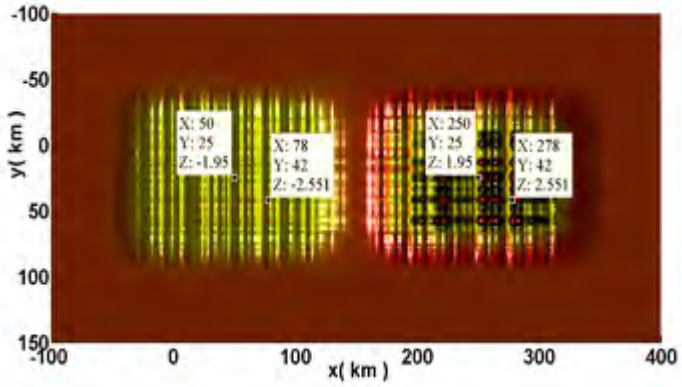

Figure 5. Top view of the stochastic submarine slump and landslide at $t^* = L/v$, showing the location of four selected gauges above the depression slump and the displaced accumulation mass movement, with the following coordinates (x, y) in km: (50, 25) and (78, 42), (250, 25) and (278, 42).

Figure 6 presents the vertical distance of the free surface elevation during the generation time at each gauge for Fr = 1, 0.8 and 0.6 at water depth h = 2 km. The Froude number indicated the duration over which the submarine slump and landslide interacts with the wave field and has a significant effect on the wave

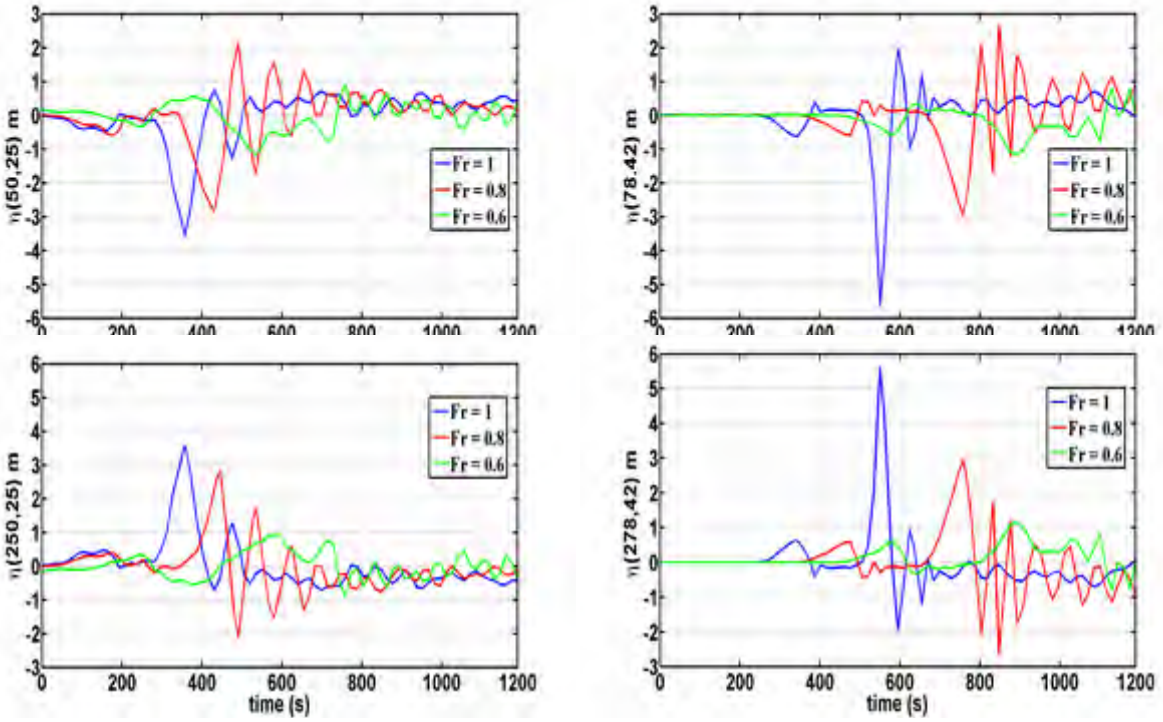

(c) Gauge at (250, 25) (d) Gauge at (278, 42)

Figure 6. Free surface elevation $\eta(x, y, t)$ at different Froude numbers along the four selected gauges located in Fig. 5 at water depth h = 2 km.

This can be observed in Fig. 6 where by decreasing the landslide Froude number, resulting in a smaller leading wave crest and tough which propagate ahead of the slump and the slide. Therefore, the Froude

number was used here to control the duration of this interaction. The maximum free surface elevation attained in Fig. (6c) at wave gauge (250, 25) for Fr = 1, 0.8 and 0.6 to 3.56, 2.83 and 0.95 m at rise time t = 357, 446 and 595 s, respectively and in Fig. (6d) at wave gauge (278, 42) reaches a maximum value of 5.63, 2.97 and 1.17 at rise time t = 550, 758 and 892 s, respectively. Figure 7 represents the normalized tsunami generated and propagated amplitude by the deterministic and stochastic submarine slump and slide source models for different values of the Froude number. It can be seen how water ahead of the front face of the slide is pushed away, creating a positive wave in the slide direction. Above the submarine slump, water is absorbed, which creates a large trough. These waveforms are generated at constant water depth h = 2 km, propagated length L = 100 km, at time t = t* where t* = L\v (time when the sea-bottom mass failure ends). It can be observed how the inclusion of the noise at the lateral slopes and to the central plateau of the submarine slump and landslide source model leads to an increase in the tsunami amplitude in addition to an increase in oscillations in the free surface elevation. In Figure 7, resonance takes place when Fr = 1, and wave focusing and amplification will occur above the spreading edge of the submarine slump and landslide (i.e. tsunami wave generation and slump and slide motion interact in a dynamic coupling). For Fr < 1, the tsunami will run away from the wave-generating submarine slump and landslide, limiting the build-up of the wave. Hence, the wave behavior is largely determined by the Froude number.

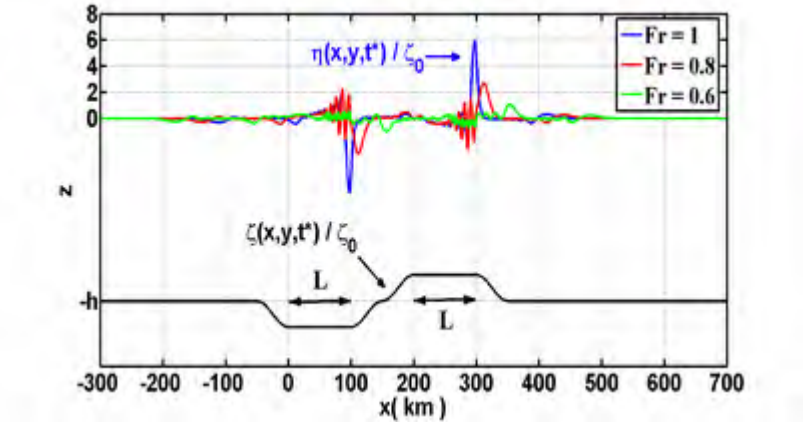

(a)

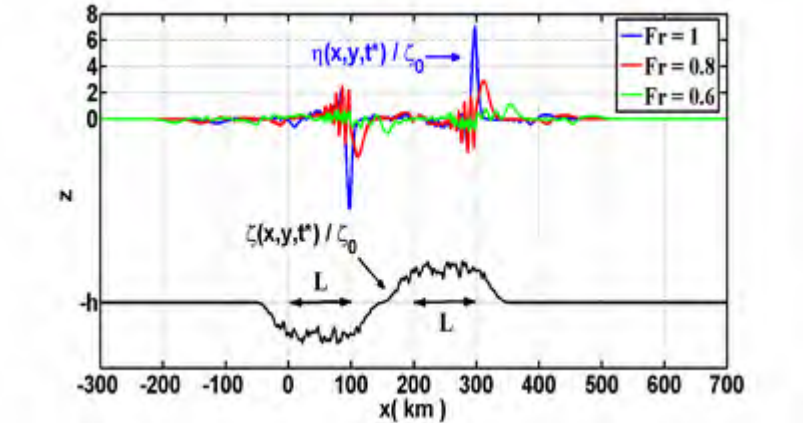

(b)

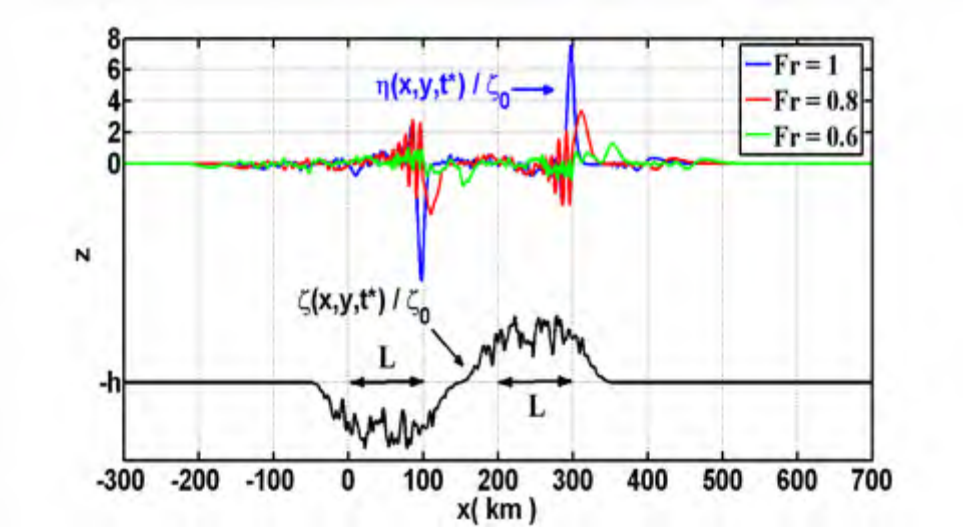

Figure 7. Comparison between the normalized tsunami amplitude generated by the deterministic (a) $\sigma_x = \sigma_y = 0$ and the stochastic submarine slump and landslide source models at (b) $\sigma_x = \sigma_y = 0.4$ and (c) $\sigma_x = \sigma_y = 0.8$ for different values of Froude number at propagated length L = 100 and water depth h = 2 km with $v_t = \sqrt{gh}$ and $t^* = L\backslash v_t$.

When the tsunami enters in the propagation regime, amplitude or leading wave height decreases with the distance from the source because of wave divergence and dispersion, which makes the wave travel outward on the surface of the ocean in all directions away from the source area as seen in Fig. 8.The leading wave crest was observed to propagate with relatively minor change in form with time, causing a train of small waves behind the main wave. The first trailing wave becomes larger than the leading one and for large propagation times, the largest amplitudes will be found in the trailing waves. For Fr < 1, the tsunami will cover much larger area than the area of the source because of wave divergence and dispersion as seen in Fig. 9. The leveling of the tsunami wave due to gravity, converts the potential energy of the water into kinetic energy resulting in dispersing wave energy over a larger area, and thereby creating a propagating wave field. The propagation of long waves in the ocean is accompanied by effects of refraction and wave scattering due to reflections by a non-uniform ocean bottom which leads to stochastization of the wave field (Fine et al. 2013).This stochastization is quite evident in the rear area in Figs. 8 and 9, where the area is filled with secondary waves and is transformed into a random wave field. Hence, the stochastic submarine slump and landslide model shows more oscillations in the propagated free surface elevation.

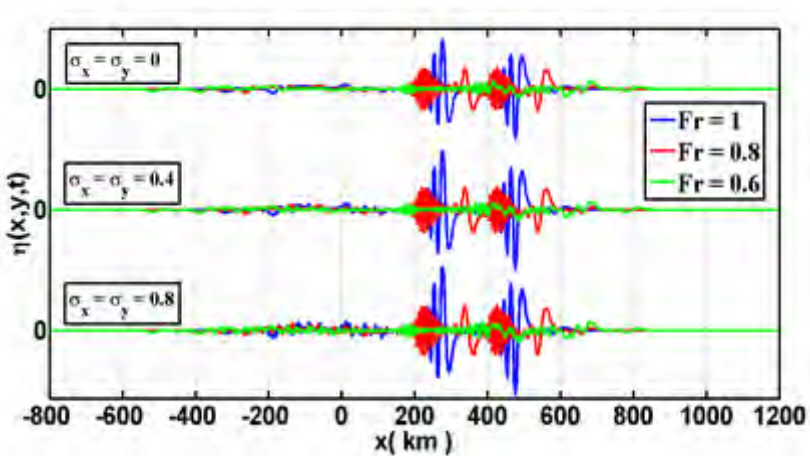

Figure 8. Normalized tsunami propagation waveforms by the deterministic and the stochastic submarine slump and landslide source models for different values of Froude number and different noise at propagated time $t = 3\ t^*$.

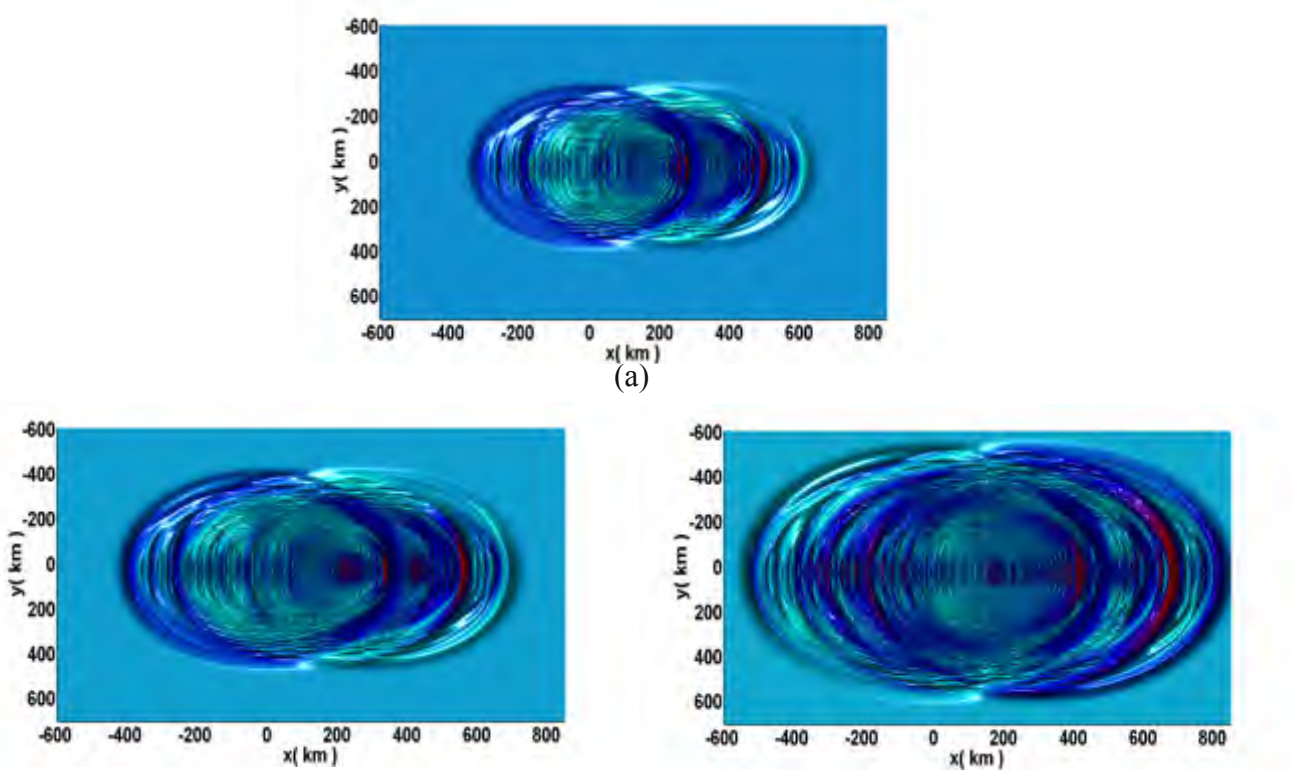

(a)

(b) (c)

Figure 9. Top views of the normalized tsunami propagation waveforms shown in Fig. 8 by the stochastic submarine slump and landslide source model at $\sigma_x = \sigma_y = 0.8$, for (a) Fr = 1 , (b) Fr = 0.8 and (c) Fr =

3.2 Displaced Water Volume and Tsunami Energy

Tsunamis are generated by water volume displacement as a result of ocean-bottom displacement due to faulting or by submarine slump and landslide due to geophysical mass flow events. We are interesting to analyze wave elevation history using the displaced water volume as a result of the deterministic and the stochastic submarine slump and landslide motions and the resulted energy of the free surface elevation. As the vertical displacement of the deterministic and stochastic submarine slump and landslide source models increases during the generation process, results in more displaced water volume in the ocean, which is proportional to the source models spreading distance as seen in Fig. 10. For Fr = 1, the displaced water volume by the deterministic submarine slump and landslide source model for propagated length L = 50 and 100 km reaches a maximum of 2.0 and 3.0 km^3, respectively , while in case of the stochastic submarine slump and landslide source model, reaches a maximum of 2.07 and 3.15 km^3. This indicates that the near–field tsunami amplitudes are roughly proportional to the source volume and deformation. It can be observed that the duration over which the submarine slump and landslide interacts with the wave field increases as the Froude number decreases. In the propagation regime, the displaced water volume remains constant as a state of conservation of energy in an open ocean.

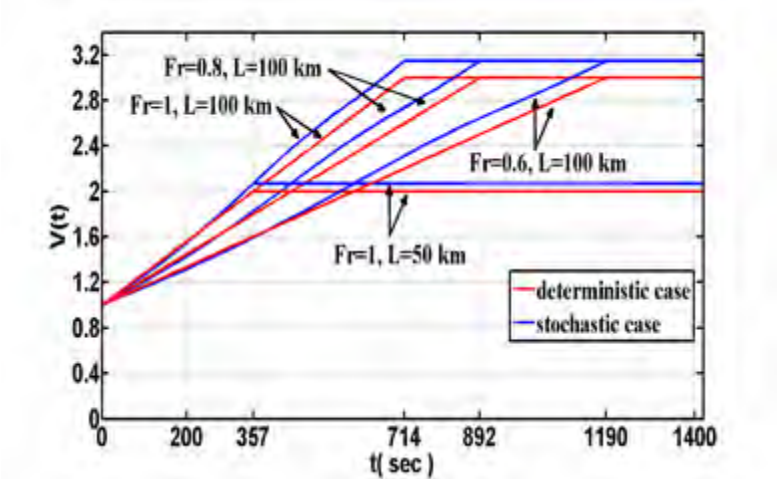

Figure 10**.** Time evolution of the displaced water volume as a result of the deterministic and the stochastic submarine slump and landslide source models to propagated lengths L = 50 and 100 km at time t = 357 and 714 sec, respectively for different Froude numbers.

For better understanding of the submarine slump and landslide generation it would be interesting to examine the energy transfer from the slump and the landslide to the water surface. Figure 11 shows the potential, kinetic and total energy vs. time induced by the deterministic and the stochastic submarine slump and landslide source models during the wave generation and propagation process for different Froude numbers. It can be seen in Fig. 11 that both the potential and kinetic energy increases during the generation region due to the submarine slump and landslide flow and hence increases the total energy. The wave energy reaches a maximum which indicates that the generated waves are mostly developed. The total energy of the maximum elevation, calculated by the deterministic submarine slump and landslide is 4.8×10^{14} , 3×10^{14} and 1.0×10^{14} J for Fr = 1, 0.8 and 0.6, respectively and due to the stochastic submarine slump and landslide yields maximum total energy of approximately 6.8×10^{14}, 4.0×10^{14} and 1.3×10^{14} J. The rate

at which the potential and kinetic energy increased depended on the value of the Froude. As the Froude number increased, the amplitude of the energy fluctuations during the constant-velocity phase also increased. Hence, the results shown in Fig. 11 indicated that the energy content of near-field tsunami depend on tsunami source deformation and the Froude number. Vol. 37, No. 1, page 1 (2018)

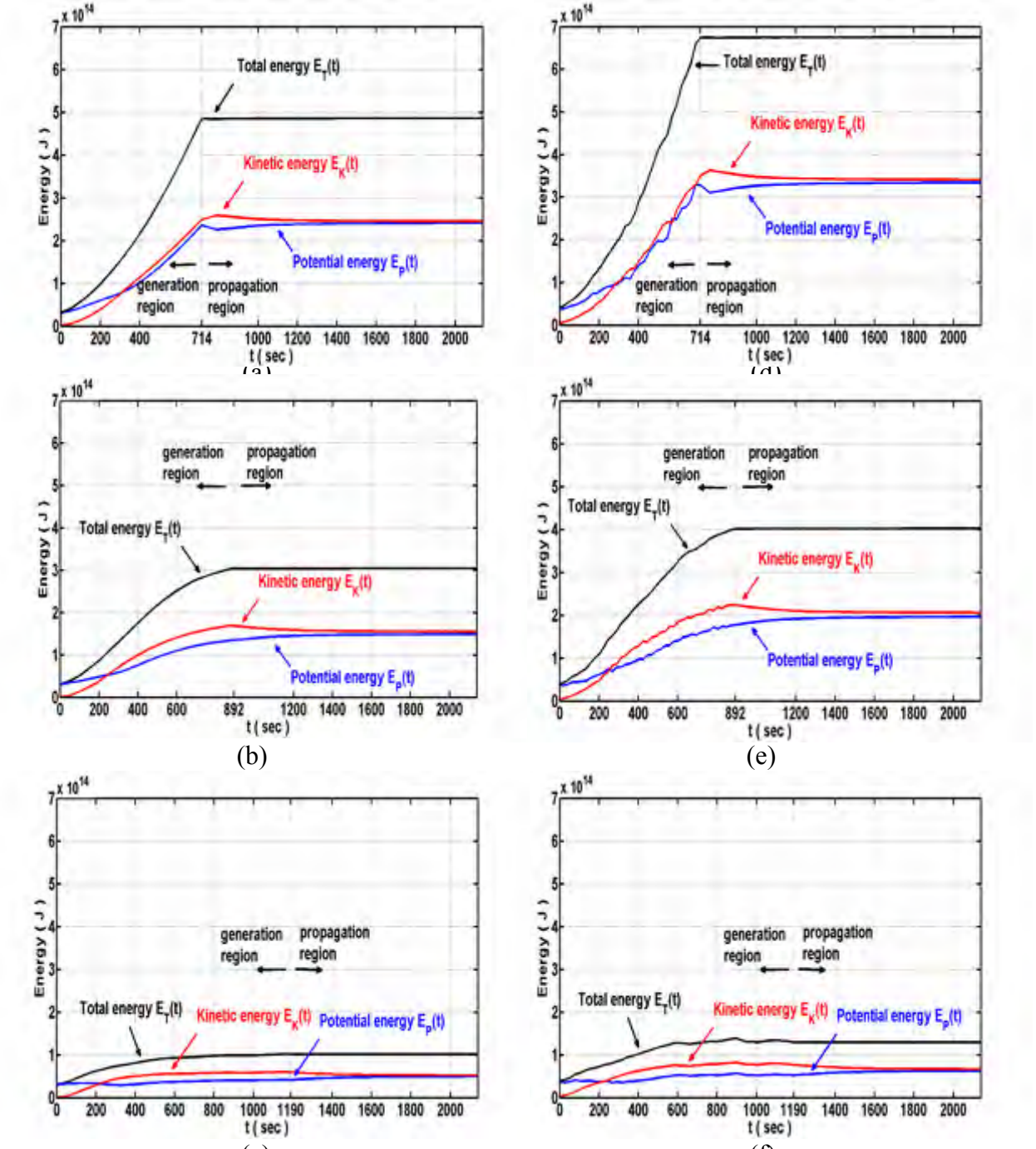

Figure 11. Energy evolution during the generation and propagation process induced by the deterministic submarine slump and landslide source model for (a) Fr = 1, (b) Fr = 0.8 and (c) Fr = 0.6, and by the stochastic submarine slump and landslide source model for (d) Fr = 1, (e) Fr = 0.8 and (f) Fr = 0.6, until propagated time $t = 3\ t^{*}$.

When the tsunami enters the propagation regime, amplitude or wave height decreases with the distance from the source because of wave divergence and dispersion, and hence decreases the potential energy, while the kinetic energy increases as seen in Fig. 11. This makes the wave travel outward on the surface of the ocean in all directions away from the source area. The potential energy resulting from the generation process is balanced with the kinetic energy of the waves which appears as an exchange between kinetic and potential energy due to the conservation of energy which was verified in the total energy. The energy of the leading wave crest was found to decrease with the propagation distance attributed to the dispersion of the wave energy and migration through the tsunami wave train (Løvholt et al. 2008). This was observed in the propagation region in Fig. 11 where the energy transfer to the trailing waves in the wave train led to the potential energy increases in the propagation region which comprises multiple amplitudes and frequency components formed immediately behind the leading wave. All curves reach an energy saturation plateau for large times, which is higher, the closer to 1 is the Froude number. Saturation is reached later for smaller Froude numbers.

It is also interesting to report previous values computed for the tsunami energy induced by landslides. Levin and Nosov (2009) estimated the energy of the tsunami waves generated by landslide of the order of 10^{16} J. Abril, and Periáñez (2015) estimated the tsunami peak energy by a submarine landslide to be equal to 4.2×10^{15} J. López-Venegas et al. (2015) calculated the potential energy of the tsunami wave produced by the landslide to be 0.95×10^{15} J and the kinetic energy to be 3.5×10^{15} inside the generation area. For tsunami energy induced by submarine earthquake, Ramadan et al. (2017) computed the tsunami maximum total energy of approximately 2.9×10^{14} J.

3.3 Average Velocity Time Series

We are interested in representing the time series of the average velocity flow rates $\bar{u}$ and $\bar{v}$, induced by the displacement of deterministic and stochastic submarine mass failure along the free surface ($z = 0$) under the effect of different Froude numbers. The time series of the average velocity components provides a clear signal of tsunami flows, where the arrival of the tsunami is indicated by the commencement of distinctive current velocity oscillations as it shows the characteristic oscillations produced by the tsunami (Lipa et al. 2011, 2012). The surface average velocity flow rates are written as $\bar{u} = \frac{Q_x}{\iint dxdy}$ and $\bar{v} = \frac{Q_y}{\iint dxdy}$, where $Q_x = \iint u dxdy$ and $Q_y = \iint v dxdy$ are called volume flow rates.

Figure 12 represents the time series of the surface average velocities $\bar{u}$ and $\bar{v}$ of the tsunami generated and propagated waves by the spreading deterministic and stochastic submarine slump and landslide source models of propagated length L = 100 km at water depth h = 2 km. It can be seen in Fig. 12 that the contribution of the randomness of the stochastic submarine slump and landslide source model affected the average velocity flow rates by distinctive oscillations. Hence, the average velocity flow rates can provide valuable information about the mass flow. In the $y-$direction, the stochastic submarine slump and landslide source model propagates instantaneously as the water surface elevation builds up rapidly, and therefore the horizontal average velocity flow rate $\bar{v}$ develops a spike with drastically frequency oscillations. The oscillations in the propagation region appear due to wave dispersion and the changes in the average velocity flow rates have minimal impacts. The peak average flow rates $\bar{u}$ reaches a maximum of 0.634, 0.856 and 0.956 m/s, for Fr = 1, 0.8 and 0.6, respectively in the case of the deterministic submarine slump and

landslide, and a maximum of 0.852, 1.138 and 1.182 m/s, in the case of the stochastic submarine slump and landslide. When the Froude number decreases, the tsunami wavelength decreases and the frequency oscillation and dispersion increases and hence increases the horizontal average surface velocities.

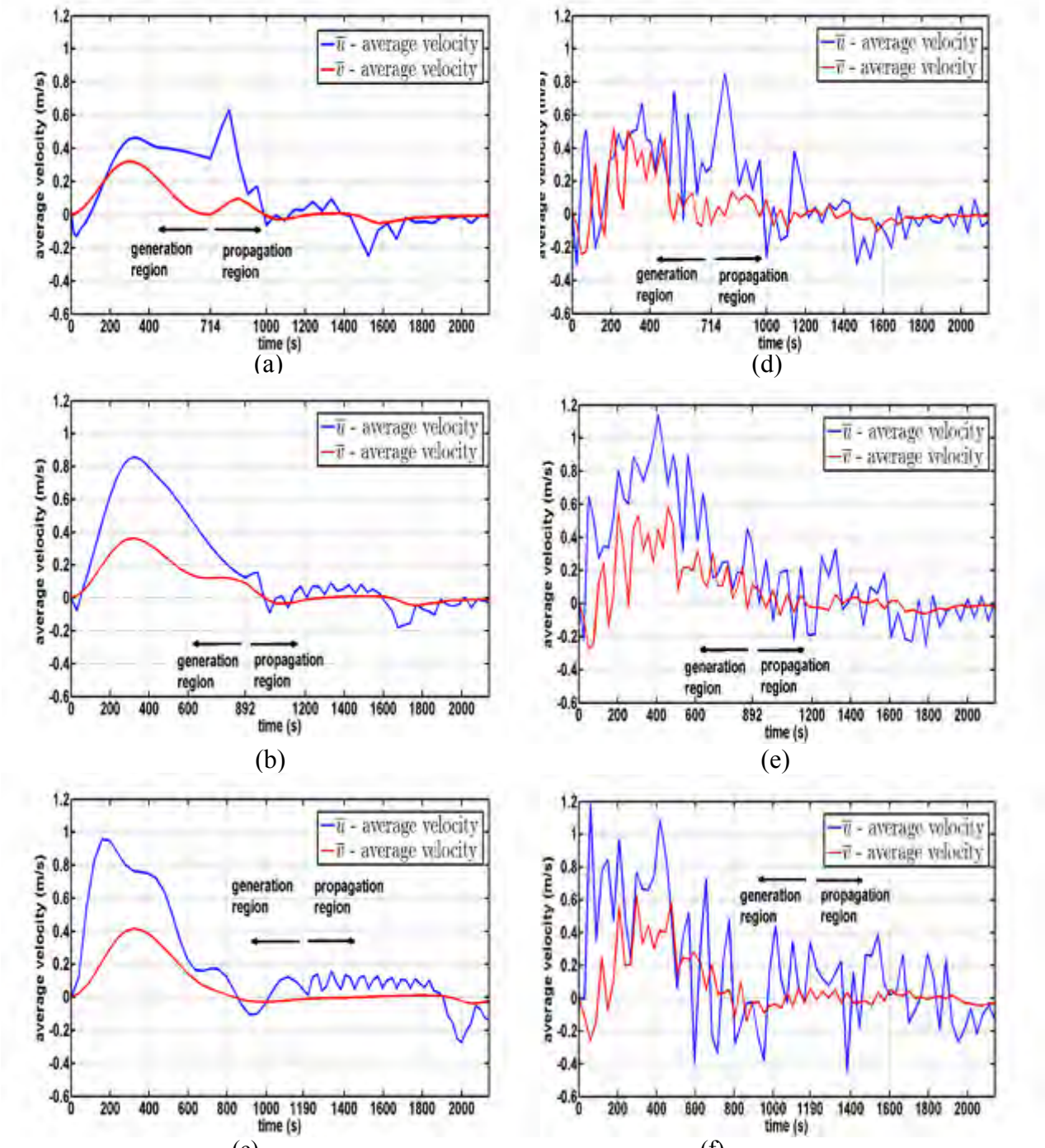

Figure 12. Time evolution of the surface average velocities ū and v̄ during the generation and propagation processes induced by the deterministic submarine slump and landslide source models for (a) Fr = 1 and (b) Fr = 0.8 and (c) Fr = 0.6, and by the stochastic submarine landslide source model for $\sigma_x = \sigma_y = 0.8$, and (d) Fr = 1, (e) Fr = 0.8 and (f) Fr = 0.6.

4. CONCLUSIONS

In this study, the tsunami distributions in the near–and far–field were investigated, resulting from a submarine slump and landslide modeled by a dynamic mass movement of a stochastic source model, driven by two Gaussian white noise processes in the x– and y–directions. We provided quantitative information by examining particular features of the displaced water volume by the stochastic submarine slump and landslide, the potential and kinetic energy and the average velocity flow rates to gain insight into the nature of the tsunami's genesis and propagation and to provide valuable information about the submarine slump and landslide. Wave gauges were measured for helping tsunami warning centers to issue or cancel warnings and to make a contribution to the improvement the warning system of tsunami arrival. Through our analysis, the following understandings and conclusions were obtained:

(1) Increasing the noise intensity will increase the amplitude of the stochastic submarine slump and landslide source model and hence increases the amplitudes and oscillations of the generated tsunami wave.

(2) The increase in the noise intensity was quite evident in the rear area of the propagated tsunami wave.

(3) When the slide velocity is similar to the tsunami phase velocity in the source area (Fr = 1), this indicated that landslide and tsunamis were coupled to generate the large tsunami heights. When the Froude number is less than one, then the tsunami will run away from the wave generating slump and landslide, limiting the build-up of the wave.

(4) The Froude number indicated the duration over which the submarine slump and landslide interacts with the wave field and has a significant effect on the wave amplitudes.

(5) The inclusion of the random noise of submarine slump and landslide deformation provided an additional and a noticeable contribution to the displaced water volume and the potential and kinetic energy of the tsunami wave.

(6) The amount of water displaced increased as the vertical movement of the deterministic and stochastic submarine slump and landslide source models increases (i.e. propagated length increases) during the generation process and then remained constant as entering the propagation regime a sort of conservation of energy.

(7) Exchange between potential and kinetic energy was achieved and reaches a total energy saturation plateau in the propagation process which is higher in the resonance state. Saturation is reached later for smaller Froude numbers.

(8) The Froude number influenced directly proportional the maximum free surface elevation and the energy and inversely the average horizontal velocities of the tsunami wave.

(9) When the Froude number deceases, this led to more widespread effects of the tsunami wave and the frequency oscillation and dispersion increases and accordingly increases the horizontal average velocity flow rates.

REFERENCES

Abril, J.M., & Periáñez, R. (2015). A Numerical Modelling Study on the Potential Role of Tsunamis in the Biblical Exodus. Journal of Marine Science and Engineering, 3(3), 745–771.

Allam, A.A., Omar, M.A. & Ramadan, K.T. (2014). Three-Dimensional Modeling of Tsunami Generation and Propagation under the Effect of Stochastic Seismic Fault Source Model in Linearized Shallow-Water Wave Theory. ISRN Applied Mathematics, doi.org/10.1155/2014/874230.

Bardet, J.-P., Synolakis, C. E., Davies, H. L., Imamura, F., & Okal, E. A. (2003). Landslide Tsunamis: Recent Findings and Research Directions. Pure Appl. Geophys., 160(3), 1793–1809.

Bernard, E. N., & Titov, V.V. (2015). Evolution of tsunami warning systems and products. Philos. Trans. R. Soc. Lond. A, 373(2053), 20140371, doi:10.1098/rsta.2014.0371.

Bondevik, S., Løvholt, F., Harbitz, C., Mangerud, J., Dawson, A., & Svendsen, J.I. (2005). The Storegga Slide tsunami—comparing field observations with numerical simulations. Marine and Petroleum Geology, 22(1), 195–208.

Brink, U. S., Geist, E. L., & Andrews, B.D. (2006). Size distribution of submarine landslides and its implication to tsunami hazard in Puerto Rico. Geophysical Research Letters, 33(11), L11307, doi: 10.1029/2006GL026125.

Choowong, M., Murakoshi, N., Hisada, K., Charusiri, P., Charoentitirat, T., Chutakositkanon, V., Jankaew, K., Kanjanapayont, P., & Phantuwongraj, S. (2008). 2004 Indian Ocean tsunami inflow and outflow at Phuket, Thailand. Marine Geology, 248(3–4), 179–192.

Constantin, A., & Germain, P. (2012). On the open sea propagation of water waves generated by a moving bed. Phil. Trans. R. Soc. A, 370 (1964), 1587–1601.

Degueldre, H., Metzger, J.J., Geisel, T., & Fleischmann, R. (2016). Random focusing of tsunami waves. Nature Physics, 12(3), 259–262.

Dias, F., Dutykh, D., O'Brien, L., Renzi, E., & Stefanakis, T. (2014). On the modelling of tsunami generation and tsunami inundation. Procedia IUTAM, 10, 338–355.

Didenkulova, I., Nikolkina, I., Pelinovsky, E. & Zahibo, N. (2010). Tsunami waves generated by submarine landslides of variable volume: analytical solutions for a basin of variable depth. Nat. Hazards Earth Syst. Sci., 10(11), 2407–2419.

Dutykh, D., & Dias, F. (2009). Energy of tsunami waves generated by bottom motion. Proc. R. Soc. A, 465(2103), 725–744, doi:10.1098/rspa.2008.0332.

Dutykh, D., Mitsotakis, D., Chubarov, L.B., & Shokin, Y.I. (2012). On the contribution of the horizontal sea-bed displacements into the tsunami generation process. Ocean Modelling, 56, 43–56.

Dutykh, D., Mitsotakis, D., Gardeil, X., & Dias, F. (2013). On the use of the finite fault solution for tsunami generation problems. Theoretical and Computational Fluid Dynamics, 27(1), 177–199.

Fine, I.V, Kulikov, E.A, & Cherniawsky, J.Y. (2013). Japan's 2011 tsunami: Characteristics of wave propagation from observations and numerical modeling. Pure and Applied Geophysics, 170(6–8), 1295–1307.

Fritz, H.M, Hager, W.H, & Minor, H.E. (2003). Landslide generated impulse waves. 2. Hydrodynamic impact craters. Experiments in Fluids 35(6), 520–532.

Fritz, H.M., Mohammed, F., & Yoo, J. (2009). Lituya Bay landslide impact generated mega-tsunami 50th anniversary. Pure and Applied Geophysics, 166(1-2), 153–175.

Fukutani, Y., Suppasri, A., & Imamura, F. (2015). Stochastic analysis and uncertainty assessment of tsunami wave height using a random source parameter model that targets a Tohoku-type earthquake fault. Stochastic Environmental Research and Risk Assessment, 29(7), 1763–1779.

Geist, E.L. (2002). Complex earthquake rupture and local tsunamis, J. Geophys. Res., 107(5), 2086–2100.

Geist, E. L. (2005). Rapid tsunami models and earthquake source parameters: far-field and local applications. ISET J. Earthq. Technol., 42(4), 127–136.

Geist, E.L. (2013). Near-field tsunami edge waves and complex earthquake rupture. Pure and Applied Geophysics, 170(9-10), 1475–1491.

Geist, E.L., (2016). Non-linear resonant coupling of tsunami edge waves using stochastic earthquake source models. Geophysical Journal International, 204(2), 878–891.

Glimsdal, S., Pedersen, G.K., Langtangen, H.P., Shuvalov, V., & Dypvik, H. (2007). Tsunami generation and propagation from the Mjølnir asteroid impact. Meteoritics & Planetary Science 42(9), 1473–1493.

Harbitz, C.B. (1992). Model simulations of tsunamis generated by the Storegga slides. Marine Geology, 105(1), 1–21.

Hassan, H.S., Ramadan, K.T. & Hanna, S.N. (2010). Generation and propagation of tsunami by a moving realistic curvilinear slide shape with variable velocities in linearized shallow-water wave theory. Engineering, 2(7), 529–549.

Hayir, A. (2006). The near-field tsunami amplitudes caused by submarine landslides and slumps spreading in two orthogonal directions. Ocean engineering, 33(5–6), 654–664.

Imamura, F., Gica, E., Takahashi, T., & Shuto, N. (1995). Numerical simulation of the 1992 Flores tsunami: interpretation of tsunami phenomena in northeastern Flores Island and damage at Babi Island. Pure Appl. Geophys. 144(3–4), 555–568.

Jiang, L. & LeBlond, P.H. (1992). The coupling of a submarine slide and the surface waves which it generates. J. Geophys. Res., 97 (C8), 12,731–12,744.

Jiang, L. & LeBlond, P.H. (1994). Three-dimensional modeling of tsunami generation due to a submarine mudslide. J. Phys., Oceanography, 24(3), 559–572.

Jamin, T., Gordillo, L., Ruiz-Chavarría, G., Berhanu M, & Falcon, E. (2015). Experiments on generation of surface waves by an underwater moving bottom. Proc. R. Soc. A 471(2178), 20150069, doi: 10.1098/rspa.2015.0069.

Kervella, Y., Dutykh, D., & Dias, F. (2007). Comparison between three-dimensional linear and nonlinear tsunami generation models. Theoretical and Computational Fluid Dynamics, 21(4), 245–269.

Levin, B., & Nosov, M. (2009). The physics of tsunami formation by sources of nonseismic origin. Physics of Tsunamis, Springer, Netherlands, 153–195.

Lin, P., Liu, X. & Zhang, J. (2015). The simulation of a landslide-induced surge wave and its overtopping of a dam using a coupled ISPH model. Engineering Applications of Computational Fluid Mechanics, 9(1), 432–444.

Lipa, B., Barrick, D., Saitoh, S.I., Ishikawa, Y., Awaji, T., & Largier, J. (2011). Garfield N. Japan tsunami current flows observed by HF radars on two continents. Remote Sensing, 3(8), 1663–1679.

Lipa, B., Isaacson, J., Nyden, B., & Barrick, D. (2012). Tsunami arrival detection with high frequency (HF) radar. Remote Sensing, 4(5), 1448–1461.

López-Venegas, A.M., Horrillo, J., Pampell-Manis, A., Huérfano, V. & Mercado, A. (2015). Advanced tsunami numerical simulations and energy considerations by use of 3D–2D coupled models: the October 11, 1918, Mona Passage Tsunami. Pure and Applied Geophysics, 172(6), 1679–1698.

Løvholt, F., Pedersen, G., & Gisler, G. (2008). Oceanic propagation of a potential tsunami from the La Palma Island. Journal of Geophysical Research, 113(C9), C09026, doi:10.1029/2007JC004603.

Løvholt, F., Pedersen, G., Bazin, S., Kühn, D., Bredesen, R.E., & Harbitz, C. (2012). Stochastic analysis of tsunami runup due to heterogeneous coseismic slip and dispersion. Journal of Geophysical Research: Oceans 117(C3), doi:10.1029/2011JC007616.

Løvholt, F., Bondevik, S., Laberg, J.S., Kim, J. & Boylan, N. (2017). Some giant submarine landslides do not produce large tsunamis. Geophys. Res. Lett., 44(16), doi:10.1002/2017GL074062.

Lynett, P., & Liu, P.L.F. (2002). A numerical study of submarine-landslide-generated waves and run-up. Proc. R. Soc. Lond. A, 458(2028), 2885–2910.

Ma, G., Kirby, J.T., & Shi, F. (2013). Numerical simulation of tsunami waves generated by deformable submarine landslides. Ocean Modelling, 69, 146–165.

Ma, G., Kirby, J.T., Hsu, T.J., & Shi, F. (2015). A two-layer granular landslide model for tsunami wave generation: Theory and computation. Ocean Modelling, 93, 40–55.

McFall, B.C., & Fritz, H.M. (2016). Physical modelling of tsunamis generated by three-dimensional deformable granular landslides on planar and conical island slopes. Proc. R. Soc. A, 472(2188), 20160052, doi: 10.1098/rspa.2016.0052.

Normark, W.R., Moore, J.G., & Torresan, M. (1993). Giant Volcano-Related Landslides and the Development of the Hawaiian Islands in Submarine Landslides: Selected Studies in the US Exclusive Economic Zone. US Geological Survey Bulletin 2002, US Department of the interior, Denver CO, 184–196.

Okal, E.A., Fryer, G.J., Borrero, J.C., & Ruscher, C. (2002). The landslide and local tsunami of 13 September 1999 on Fatu Hiva (Marquesas Islands; French Polynesia). Bulletin de la Société Géologique de France, 173(4), 359–367.

Omar, M.A., Allam, A.A., & Ramadan, K.T. (2012). Generation and Propagation of Tsunami Wave under the Effect of Stochastic Bottom. International Conference on Mathematics Trends and Development (ICMTD12).

Omar, M.A., Ramadan, K.T., & Allam, A.A. (2014). Linearized Shallow-water Wave Theory of Tsunami Generation and Propagation by Three-dimensional Stochastic Seismic Bottom Topography. Research Journal of Applied Sciences, Engineering and Technology 7(19), 4035–4055.

Omar, M.A., Ramadan, K.T. & Allam, A.A. (2017). Tsunami Generation and Propagation by a Curvilinear Stochastic Spreading Seismic Faulting in Linearized Water Wave Theory. Journal of Earthquake and Tsunami, 11(3), 1750005, doi: 10.1142/S1793431117500051.

Ramadan, K.T., Hassan, H.S., & Hanna, S.N. (2011). Modeling of tsunami generation and propagation by a spreading curvilinear seismic faulting in linearized shallow-water wave theory. Applied Mathematical Modelling, 35(1), 61–79.

Ramadan, K.T., Omar, M.A. & Allam, A.A. (2014). Modeling of tsunami generation and propagation under the effect of stochastic submarine landslides and slumps spreading in two orthogonal directions. Ocean Engineering, 75, 90–111.

Ramadan, K. T. (2014). Tsunami Generation and Propagation by a Curvilinear Stochastic source fault model in Linearized Shallow-Water Wave Theory. European Journal of Scientific Research, 124(3), 328–358.

Ramadan, K.T., Omar, M.A., & Allam, A.A. (2017). Tsunami Energy, Ocean-Bottom Pressure, and Hydrodynamic Force from Stochastic Bottom Displacement. Pure and Applied Geophysics 174(3), 1315–1330.

Ramadan, K. T., Allam, A. A., & Omar, M. A. (2015). Near-and far-field tsunami amplitudes by a moving curvilinear stochastic submarine slide shape based on linearized water wave theory. Ocean Engineering, 109, 34–59.

Ranguelov, B., Tinti, S., Pagnoni, G., Tonini, R., Zaniboni, F., & Armigliato, A. (2008). The nonseismic tsunami observed in the Bulgarian Black Sea on 7 May 2007: was it due to a submarine landslide ?. Geophysical Research Letters, 35(18), 1–5.

Ruiz, J.A., Fuentes, M., Riquelme, S., Campos, J., & Cisternas, A. (2015), Numerical simulation of tsunami runup in northern Chile based on non-uniform k− 2 slip distributions. Natural Hazards, 79(2), 1177–1198.

Ruff, L. J. (2003). Some Aspects of Energy Balance and Tsunami Generation by Earthquakes and Landslides, Pure and Applied Geophysics. 160, 2155–2176.

Saito, T., & Furumura, T. (2009). Three-dimensional tsunami generation simulation due to sea-bottom deformation and its interpretation based on the linear theory. Geophysical Journal International, 178(2), 877–888.

Saito, T. (2013). Dynamic tsunami generation due to sea-bottom deformation: Analytical representation based on linear potential theory. Earth, Planets and Space, 65(12), 1411–1423.

Samaras, A.G., Karambas, T.V., & Archetti, R. (2015). Simulation of tsunami generation, propagation and coastal inundation in the Eastern Mediterranean. Ocean Science, 11(4), 643–655.

Satake, K., & Tanioka, Y. (2003). The July 1998 Papua New Guinea Earthquake: mechanism and quantification of unusual tsunami generation. Pure and Applied Geophysics 160, 2087–2188.

Schwab, W.C., Danforth, W.W., & Scanlon, K.M. (1993). Tectonic and Stratigraphic Control on a Giant Submarine Slope Failure: Puerto Rico Insular Slope: Selected Studies in the US Exclusive Economic Zone. US Geological Survey Bulletin 2002, US Department of the interior, Denver CO, 60–68.

Synolakis, C.E., Bardet, J.P., Borrero, J.C., Davies, H.L., Okal, E.A., Silver, E.A., Sweet, S. & Tappin, D.R. (2002). The slump origin of the 1998 Papua New Guinea tsunami. Proceedings of the Royal Society of London A: Mathematical, Physical and Engineering Sciences, 458(2020), 763–789.

Tang, L., Titov, V.V., Bernard, E.N., Wei, Y., Chamberlin, C.D., Newman, J.C., Mofjeld, H.O., Arcas, D., Eble M.C., Moore, C., Uslu, B., Pells, C., Spillane, M., Wright, L., & Gica, E. (2012). Direct energy estimation of the 2011 Japan tsunami using deep-ocean pressure measurements. J.Geophys. Res. 117(C8), C08008, doi: 10.1029/2011JC007635.

Tappin, D.R., Watts, P. & Grilli, S.T. (2008). The Papua New Guinea tsunami of 17 July 1998: anatomy of a catastrophic event. Natural Hazards and Earth System Science, 8(2), 243–266.

Tinti, S., & Bortolucci, E. (2000). Energy of water waves induced by submarine landslides. Pure and Applied Geophysics, 157(3), 281–318.

Tinti, S., Pagnoni, G., Zaniboni, F. (2006). The landslides and tsunamis of the 30th of December 2002 in Stromboli analysed through numerical simulations. Bulletin of Volcanology, 68(5), 462–479.

Todorovska, M.I., & Trifunac, M.D. (2001). Generation of tsunamis by a slowly spreading uplift of the sea floor. Soil Dynamics and Earthquake Engineering, 21(2), 151–167.

Todorovska, M.I., Hayir, A., & Trifunac, M.D. (2002). A note on tsunami amplitudes above submarine slides and slumps. Soil Dyn. Earthq. Eng. 22(2), 129–141.

Trifunac, M.D., Hayir, A., & Todorovska, M.I. (2002a). A note on the effects of nonuniform spreading velocity of submarine slumps and slides on the near-field tsunami amplitudes. Soil Dyn. Earthq. Eng., .22(3), 167–180.

Trifunac, M.D., Hayir, A., & Todorovska, M.I. (2002b). Was Grand Banks event of 1929: a slump spreading in two directions. Soil Dyn. Earthq. Eng., 22(5), 349–360.

Trifunac, M.D., Hayir, A., & Todorovska, M.I. (2003). A note on tsunami caused by submarine slides and slumps spreading in one dimension with nonuniform displacement amplitudes. Soil Dyn. Earthq. Eng., 23(3), 41–52.

Yavari-Ramshe, S., & Ataie-Ashtiani, B. (2016). Numerical modeling of subaerial and submarine landslide-generated tsunami waves—recent advances and future challenges. Landslides, 13(6), 1325–1368.

Watts, P., Grilli, S. T., Tappin, D. R., & Fryer, G. J. (2005). Tsunami generation by submarine mass failure. II: Predictive equations and case studies. Journal of Waterway, Port, Coastal and Ocean Engineering, 131(6), 298–310.

Whittaker, C., Nokes, R. & Davidson, M. (2015). Tsunami forcing by a low Froude number landslide. Environmental Fluid Mechanics, 15(6), 1215–1239.

Zhao, X., Wang, B. & Liu, H. (2012). Characteristics of tsunami motion and energy budget during runup and rundown processes over a plane beach. Physics of Fluids, 24(6), 062107.